

# PHOTORESIST EFFECTS ON WAFER CHARGING CONTROL: CURRENT-VOLTAGE CHARACTERISTICS MEASURED WITH CHARM-2 MONITORS DURING HIGH-CURRENT As<sup>+</sup> IMPLANTATION

Michael Current (michael\_current@amat.com) and

Majeed A. Foad (majeed\_foad@amat.com), Applied Materials, Santa Clara, CA,

Steve Brown (stephen.brown@Microchip.com), Microchip Technology, Tempe, AZ,

Wes Lukaszek (lukaszek@CHARM-2.com), Wafer Charge Monitors, Woodside, CA,

Michael C. Vella (mcvella@lbl.gov), Electro-Graph, Carlsbad, CA.

**Abstract** -The effects of ion energy, accumulated dose, photoresist coverage and patterning were studied for As<sup>+</sup> implants at 40, 60 and 120 keV and total doses from  $1 \times 10^{14}$  to  $10^{16}$  As/cm<sup>2</sup>. The effect of photoresist coverage, ion energy and dose on positive and negative potentials and j-V characteristics are presented. J-V data are fit with a beam plasma model that describes both positive and negative charging with a consistent set of plasma parameters.

## I. INTRODUCTION

The effects of the presence of photoresist (PR) on wafers, although a near-universal condition for CMOS device wafers, has received only scant attention in studies of wafer charging effects during ion implantation. Studies using CHARM<sup>®</sup>-2 sensors with half-wafer coverage of photoresist showed strong shifts towards more positive current density-voltage (j-V) characteristics for the sensors covered with PR compared to sensors in die exposed to the ion beam [1]. Similar effects were seen with CV measurements of oxide traps for capacitors either under or near a half-wafer PR coverage [2]. An early study of the effects of PR patterning near oxide capacitors [3], reported severe increases in oxide failures for capacitors in contact with or surrounded by PR fields as well as for PR patterns which blocked conduction paths to the major grounding paths, such as metal ring clamps. A recent study showed strong degradation of oxide capacitor yield for BF<sub>2</sub> implants with PR covering, or nearly covering, polysilicon capacitors [4]. PR patterning on CHARM<sup>®</sup>-2 sensors for 80 keV As implants and no charge control system operating showed strong positive shifts in +j-V characteristics for charge collection electrodes covered with PR [5]. This study also showed that shifts in the net j-V characteristics change as the implant proceeds, with the largest effects occurring early in the implant when the PR outgassing rate is high [6].

## II. EXPERIMENTAL DETAILS

This work explores the effects of dose, ion energy and PR coverage on charge collection electrodes of CHARM<sup>®</sup>-2 sensors. The PR patterns were designed to provide a decomposition of PR patterns used on CMOS device wafers with both area and edge-intensive structures [7]. Results discussed in this paper are for the area structures. The PR pattern types are: (1) PR on the die and extending up over the Al charge collection electrodes (CCE) for a distance of 3 μm (an "IN" pattern), (2) PR surrounding the CCEs from a distance of 3 μm (an "OUT" pattern), (3) PR covering the die, including the CCEs, except for the Al probe pads (a

"COVERED" (COV) pattern) and (4) PR covering the die, including most of the CCE area, except for a 3 μm wide edge on the CCE and a 3 μm space around CCE and the Al probe pads (an "EDGE" pattern) (Fig. 1).

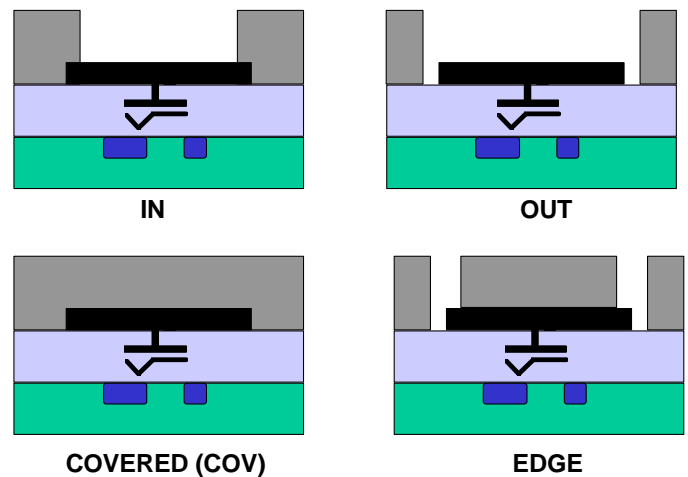


Fig 1: Photoresist pattern types on CHARM<sup>®</sup>-2 charging sensors. The overlap and gap distances are 3 μm.

The implants were done with As beams in a 9500xR implanter at energies of 40, 60 and 120 keV. Beam current was 10 mA, with beam current densities of  $\approx 1$  mA/cm<sup>2</sup>. The dose ranged from  $10^{14}$  to  $10^{16}$  As/cm<sup>2</sup>. The plasma flood source (PFS) [8] was operated in the accel-decel mode with an Ar arc current of 4 A and a -10 V guidetube bias. These PFS settings provide j-V characteristics within the range of the CHARM<sup>®</sup>-2 sensors. Wafer size was 150mm.

## III. RESULTS

### 3.1 Pattern effects

The behavior of certain j-V characteristics and the highest floating potentials observed in this study were dominated by the PR pattern type. The positive surface voltages were highest for COV and EDGE patterns (see the even numbered rows in Fig. 2a) and significantly lower for IN and OUT structures (odd numbered rows in Fig. 2a). The common feature of the COV and EDGE pattern is the complete, or nearly complete, coverage of the CCEs with PR.

For the negative surface voltages measured with the "last pass" sensors, the most negative voltages were measured

for sensors with EDGE and OUT patterns (even number columns in Fig 2b). The IN and COV patterns (odd numbered columns in Fig 2b) produced far less negative surface voltages. The common feature of the EDGE and OUT patterns is that,

although the PR coverage level is nearly complete for the EDGE and zero for the OUT pattern, both patterns disconnect the CEEs from the “field” resist area.

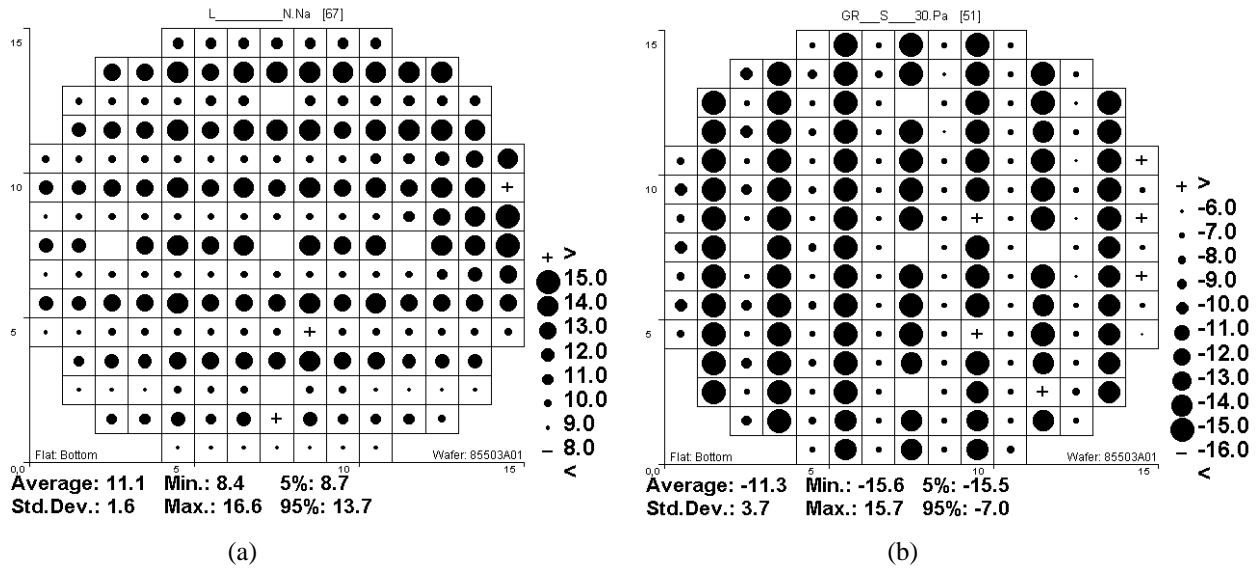


Fig 2. Positive (a) and negative (b) potentials for 120 keV As implants at a dose of  $2 \times 10^{15}$  As/cm<sup>2</sup>. The high positive potentials (large dots) are for the rows of COV and EDGE patterns. The beam path over the wafer is right to left and a slight decrease in positive surface potentials can be seen along the beam path. The most negative potentials (large dots) are for the columns of OUT and EDGE patterns. The pattern of negative potentials is uniform over the wafer in this case.

### 3.2 Dose and cross-wafer trends

CHARM CEEs that are *not* tied to the Si wafer substrate through a resistor or a diode record the surface potentials during the last few passes through the ion beam (the repeat cycle for beam passes is  $\cong 50$  ms). At a dose of  $10^{14}$  As/cm<sup>2</sup>, when the PR outgassing is occurring throughout the implant cycle [6], all negative potential sensors saturated at -17 V. For implants at  $\cong 1 \times 10^{15}$  As/cm<sup>2</sup>, strong variation in the negative, “last pass” surface potentials were observed for the IN pattern, both as a function of dose and across the wafer along the direction of the ion beam path (Fig. 3). At a dose of  $10^{15}$  As/cm<sup>2</sup>, the PR outgassing rate is dropping and a variation in surface potential was seen across the wafer, going more negative along the beam path across the wafer (right to left in Fig. 2, a top to bottom sequence in Fig. 3).

For increasing dose, positive j-V characteristics shifted in a monotonic fashion (Fig. 4). The largest negative j-V current flow was also at the highest dose.

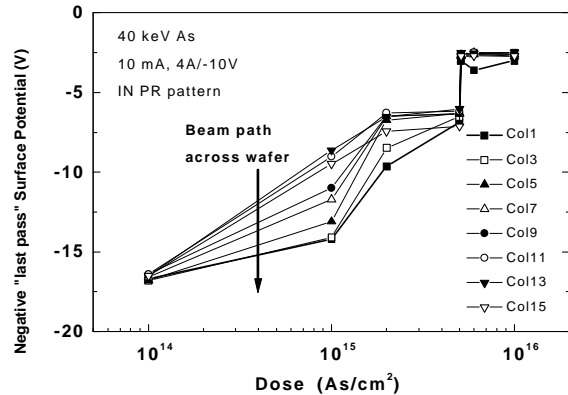


Fig 3. Variation of negative potentials with dose for the IN PR pattern, for 40 keV As implants, showing effects of the pressure “plume” as the beam passes over the wafer for doses less than  $2 \times 10^{15}$  As/cm<sup>2</sup>. Doses higher than  $5 \times 10^{15}$  As/cm<sup>2</sup> were done with a second implant cycle of  $5 \times 10^{15}$  As/cm<sup>2</sup> with the PR from the previous implants in place. All sensors were saturated at -17 V for  $5 \times 10^{14}$  As/cm<sup>2</sup>.

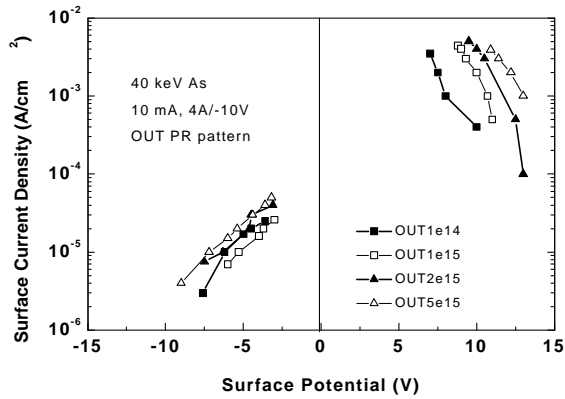


Fig. 4. Dose effects for 40 keV As with the OUT PR pattern (Note: The sign of  $j$  is reversed for  $V < 0$  for figs. 4-8).

### 3.3 Ion energy effects

The  $j$ - $V$  characteristics of the net current are obtained by combining the current signal from a number of CEEs which are tied to the Si substrate with resistors of various resistance values [9].  $J$ - $V$  characteristics vary strongly with ion energy, dose, the presence of PR on the wafer and the type of PR pattern. For 40 keV As implants (Fig. 5), the principal effect of PR is to shift the positive  $j$ - $V$  curves to higher voltages and currents, with no change in the much smaller, negative current.

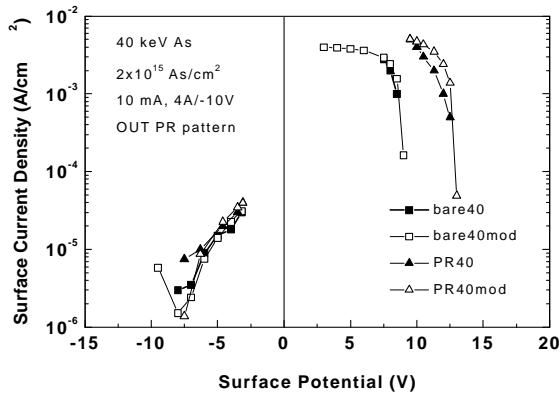


Fig. 5. Current density-voltage characteristics for 40 keV As beams with and without PR coverage for the OUT PR pattern. The  $j$ - $V$  fits to a beam plasma model (Section IV) are labeled as “mod”.

Three effects are evident in the 120 keV As implants (Fig. 6). The bare wafer floating potentials (the positive voltages above which no net positive current flows from the beam/PFS plasma to the wafer) increase slightly. The

presence of PR on the wafer further shifts the positive current to higher values. And the strong positive current flows from the beam drive an increase in the negative currents.

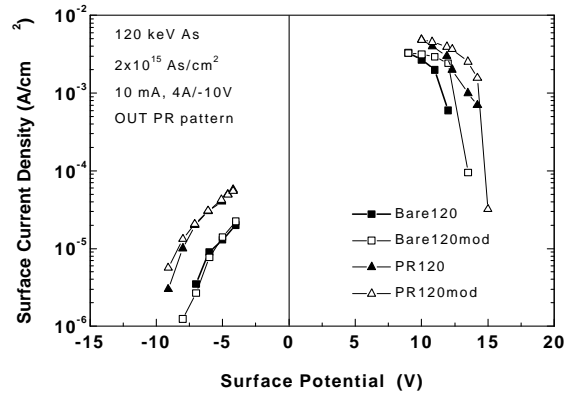


Fig. 6. Current density-voltage characteristics for 120 keV As beams with and without PR coverage for the OUT PR pattern. The  $j$ - $V$  fits to a beam plasma model (Section IV) are labeled as “mod”.

When the  $j$ - $V$  characteristics for the various PR patterns are scaled by the area of Al metal exposed to the As beam, either CEEs and/or probe pads, positive  $j$ - $V$ 's fall onto a common curve for 40 keV As beams (Fig. 7). However the negative  $j$ - $V$ 's vary with pattern type. The highest negative currents per exposed metal area are seen the patterns when the PR completely (COV) or nearly (EDGE) covers the CCEs. The COV patterns still have the Al probe pads exposed to the As beam.

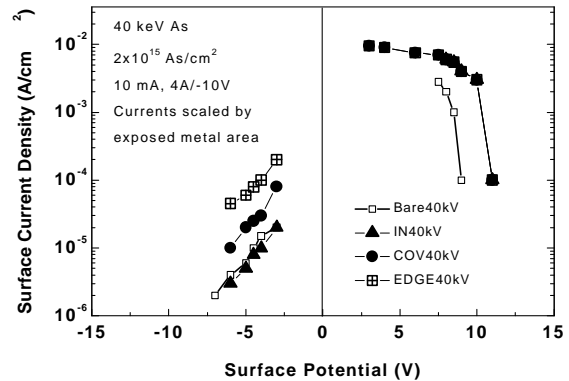


Fig 7. Net current flows for 40 keV As implants with bare and PR patterned CHARM sensors, where the measured current density is scaled by the metal area exposed to the As beam.

For 120 keV As beams (Fig. 8), both the positive and negative  $j$ - $V$  characteristics, when scaled by the exposed metal area, show different behavior for different PR pattern types.

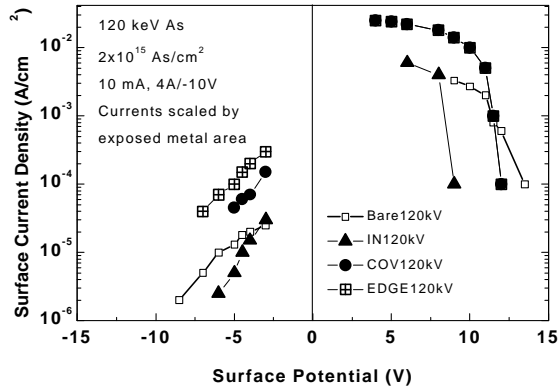


Fig 8. Net current flows for 120 keV As implants with bare and PR patterned CHARM sensors, where the measured current density is scaled by the metal area, either CEEs or probe pads, exposed to the As beam.

#### IV. DISCUSSION

The net current to the wafer when the ion beam is passing over the wafer,  $j_{net}$ , is [10]:

$$j_{net} = j_{ib}(1+\gamma) + j_{ip} - j_e \quad (1)$$

TABLE 1: Beam-plasma parameters (OUT PR pattern)

Dose =  $2 \times 10^{15}$  As/cm<sup>2</sup>,  $j_{ib} = 1$  mA/cm<sup>2</sup>,  $n_{ib} \approx 1.5 \times 10^8$  i/cm<sup>3</sup>

Energy (keV)	$n_{ip}$ (i/cm <sup>3</sup> )		$T_e$ (eV)		$\gamma$		$\Phi_p$ (V)	
	Bare	PR	Bare	PR	Bare	PR	Bare	PR
40	$7.8 \times 10^8$	$1.1 \times 10^9$	1.68	2.60	3.2	5.5	9.0	13.0
60	$7.8 \times 10^8$	$8.3 \times 10^8$	1.68	2.68	1.1	3.4	6.8	11.4
120	$7.8 \times 10^8$	$1.3 \times 10^9$	1.71	3.09	2.6	4.9	13.5	15.3

The PR fit parameters show a strong increase in plasma density and electron temperature, plus qualitatively an energy effect at 60 keV. The increase in varying  $n_{ip}$  suggests beam ionization of gas from the PR. The increase in  $T_e$  is consistent with beam ionization, since the energy of product electrons is relatively high, and increases with energy. Given that the secondary coefficient is also higher with PR, the general effect is to increase positive j-V onto the wafer under the ion beam. The negative j-V is an effect, created by the return current flowing from the wafer, through the “charge control” plasma at the edges of the beam. Fuller understanding of the j-V characteristics for diverse PR patterns moves beyond machine characterization and into the regime of CMOS process yield evaluation; combining device design rules, PR characteristics and machine conditions.

#### REFERENCES

1. W. Lukaszek, S. Reno, R. Bammi, Ion Implantation Technology-96, eds. E. Ishida et al., IEEE 96TH8182 (1997) 89-92.
2. D. Park, C.Hu. Ion Implantation Technology-96, eds. E. Ishida et al., IEEE 96TH8182 (1997) 93-95.

where  $j_{ip}$  is the plasma ion current density,  $j_e$  is the net electron current flow and  $\gamma$  is the ratio of secondary negative charges leaving the wafer per incident fast ion. Using plasma quasineutrality and assuming a Boltzman electron temperature,  $T_e$ , Eq. 1 becomes,

$$j_{net} = j_{ib}(1+\gamma) + j_{ip} [1 - (1+n_{ib}/n_{ip}) \dots * 34.2 * [A_p]^{1/2} * e^{((V-\Phi_p)/T_e)}] \quad (2)$$

where  $n_{ib}/n_{ip}$  is the ratio of beam to plasma ion density,  $A_p$  is the mass of the plasma ions,  $V$  is the wafer surface potential and  $\Phi_p$  is the beam plasma potential.

Positive j-V characteristics are described by Eq. 2; negative j-V's by setting the ion beam term,  $j_{ib}(1+\gamma)$ , to zero. The positive j-V data were fit by varying  $n_{ip}$ ,  $\Phi_p$  and  $\gamma$ , given that  $T_e$  was obtained from the slope of the negative j-V's. The energy dependence of these key parameters are listed in Table 1 for the case of the OUT PR pattern. For the bare wafers,  $n_{ip}$  and  $T_e$  were insensitive to implant energy, suggesting that plasma was dominated by the flood. The secondary coefficient did show some dependence on implant energy, as did the inferred plasma potential, which is affected by the energy of secondary electrons.

3. R. Tong, P. McNally, (IJET-84), Nucl. Instr. Meth B6 (1985) 376-381.
4. K. Bala, J. Hoepfner, H. Tanimoto, S. Takedai, S. Sugiura, B. El-Kareh, Ion Implantation Technology-96, eds. E. Ishida et al., IEEE 96TH8182 (1997)49-52.
5. W. Dixon, W. Lukaszek, C. Heden, Ion Implantation Technology-96, eds. E. Ishida et al., IEEE 96TH8182 (1997) 85-89.
6. T.C. Smith, in Ion Implantation Science and Technology, ed. J.F. Ziegler, Ion Implantation Technology Co., Yorktown, NT, USA (1996) 629-673.
7. W. Lukaszek, M.I. Current, these proceedings.
8. H. Ito, M.I. Current, Ion Implantation Technology-96, eds. E. Ishida et al., IEEE 96TH8182 (1997) 432-435.
9. Wafer Charging Monitors, 127 Marine Road, Woodside, CA 940662 USA.
10. M.I. Current, M.C. Vella, W. Lukaszek, Ion Implantation Technology-96, eds. E. Ishida et al., IEEE 96TH8182 (1997) 53-56.
11. K. Yashima, Japan Soc. Appl. Phys. (1992) 30a-SZK-1.